ISSN 1063-7834, Physics of the Solid State, 2019, Vol. 61, No. 3, pp. 345–349. © Pleiades Publishing, Ltd., 2019.
Russian Text © D.A. Balaev, A.A. Dubrovskiy, S.S. Yakushkin, G.A. Bukhtiyarova, O.N. Martyanov, 2019, published in Fizika Tverdogo Tela, 2019, Vol. 61, No. 3, pp. 478–482.

MAGNETISM

Temperature of the Magnetic Ordering of the Trivalent Iron Oxide ε-Fe_2O_3

D. A. Balaev[a, *], A. A. Dubrovskiy[a], S. S. Yakushkin[b], G. A. Bukhtiyarova[b], and O. N. Martyanov[b]

[a] *Kirensky Institute of Physics, Krasnoyarsk Scientific Center, Siberian Branch, Russian Academy of Sciences, Krasnoyarsk, 660036 Russia*

[b] *Boreskov Institute of Catalysis, Siberian Branch, Russian Academy of Sciences, Novosibirsk, 630090 Russia*

**e-mail: dabalaev@iph.krasn.ru*

Received October 11, 2018

Abstract—The trivalent iron oxide ε-Fe_2O_3 is a fairly rare polymorphic iron oxide modification, which only exists in the form of nanoparticles. This magnetically ordered material exhibits an intriguing magnetic behavior, specifically, a significant room-temperature coercivity H_C (up to ~20 kOe) and a magnetic transition in the temperature range of 80–150 K accompanied by a sharp decrease in the H_C value. Previously, the temperature of the transition to the paramagnetic state for ε-Fe_2O_3 was believed to be about 500 K. However, recent investigations have shown that the magnetically ordered phase exists in ε-Fe_2O_3 also at higher temperatures and, around 500 K, another magnetic transition occurs. Using the data on the magnetization and temperature evolution of the ferromagnetic resonance spectra, it is shown that the temperature of the transition of ε-Fe_2O_3 particles 3–10 nm in size to the paramagnetic state is ~850 K.

DOI: 10.1134/S1063783419030053

1. INTRODUCTION

The trivalent iron oxide ε-Fe_2O_3 is a magnetic material with unique properties, which was reliably characterized first in 1998. [1]. It exists in the form of nanoparticles up to ~25–40 nm in size [1–11] or nanowires up to ~100 nm in size [10–19] characterized by a significant room-temperature coercivity (~20 kOe and higher) and absorption of millimeter electromagnetic waves [10, 11, 16], which opens new prospects for application [20–22]. The ε-Fe_2O_3 nanoparticles are formed, as a rule, in the SiO_2 matrix using the modified sol–gel technique [1, 3–5, 8, 13, 23, 24] and silica gel impregnation [25, 26]. In addition, the ε-Fe_2O_3 particles can form in a K_2O–Al_2O_3–B_2O_3 glass matrix [27].

The ε-Fe_2O_3 compound has an orthorhombic noncentrosymmetric structure (sp. gr. $Pna2_1$) at room temperature. As was shown in [2, 9], in the temperature range from ~150 to ~500 K, the ε-Fe_2O_3 magnetic structure can be considered to be collinear ferrimagnetic (iron atoms are localized in four nonequivalent positions; the intersublattice coupling is antiferromagnetic and directed along the *c* axis [9]). It is the hard-magnetic phase. In the temperature range of 80–150 K, a magnetic transition in ε-Fe_2O_3 occurs [2, 6, 8–11, 14, 15, 17, 18, 24, 28–30], which is accompanied by a significant decrease in the coercivity. At low (below 80 K) temperatures, the ε-Fe_2O_3 magnetic structure is characterized as incommensurate [2, 9, 30]. According to another point of view [7, 8], in the range of 80–150 K, the ε-Fe_2O_3 compound undergoes a metamagnetic transition from a canted antiferromagnetic structure (weak ferromagnetism) to another structure with different cant angle.

It has been believed for a long time that the transition from the paramagnetic to magnetically ordered state in ε-Fe_2O_3 occurs around ~500 K. The authors of [30], using the magnetic measurements and neutron diffraction, elucidated the picture of the magnetic state in the iron oxide ε-Fe_2O_3. In the authors' opinion, the transition from the paramagnetic to magnetically ordered state occurs at T_{N1} ~ 850 K, rather than at 500 K. The new magnetic phase, which exists in the range of 500–850 K, is soft-magnetic (its coercivity is no higher than 0.5 kOe) and the magnetization is lower than in the hard-magnetic phase (150–500 K). In [30], the description of the magnetic phase in the range of $T_{N2} < T < T_{N1}$ was reduced to the fact that, at T_{N1} ~ 850 K, two magnetic iron sublattices are ferrimagnetically ordered and, at a temperature of T_{N2} ~ 500 K, the other two iron sublattices are ferrimagnetically ordered; i.e., below 500 K, there are four ferrimagnetic sublattices.

Note that, previously, sufficiently high temperatures of magnetic ordering were also detected in the ε-Fe_2O_3 compound [3, 31, 32]. On the one hand, this

behavior was interpreted as a specific feature of the extremely small ε-Fe_2O_3 particles [31, 32]. On the other hand, it is well known that ε-Fe_2O_3 can rarely be obtained without admixtures of another polymorph (hematite Fe_2O_3) and the detected high temperature of the magnetic transition is probably caused by the presence of hematite (T_N ~ 950 K for bulk samples). The data reported in this study are indicative of the fact that the ε-Fe_2O_3 compound undergoes a transition to the paramagnetic state at a temperature about 850 K, which is consistent with the conclusions made in [30]. This is demonstrated by the static magnetic measurements and ferromagnetic resonance (FMR).

2. EXPERIMENTAL

The samples containing ε-Fe_2O_3 nanoparticles in a silica gel matrix were formed from iron(II) sulfates by incipient wetness impregnation followed by drying and calcining in air at 900°C [25, 33]. Here, we report the data for the samples containing 0.74 and 3.4 wt % of iron, which are hereinafter referred to as 05FS and 3FS, respectively. The average ε-Fe_2O_3 particle sizes, according to the high-resolution transmission electron microscopy images obtained on a JEOL JEM-2010 microscope at an accelerating voltage of 200 kV, were 3.4 and 3.8 nm for samples 05FS and 3FS, respectively. The obtained images show that the interplanar spacings are consistent with the parameters observed in the of ε-Fe_2O_3 X-ray diffraction patterns. The particle size distribution histograms for the investigated samples are shown in the inset in Fig. 1.

The X-ray diffraction analysis revealed the ε-Fe_2O_3 phase only in sample 3FS, since the ε-Fe_2O_3 oxide content in sample 05FS is small. The iron oxide β phase was identified by Mössbauer spectroscopy. The analysis of the Mössbauer spectra showed that ε-Fe_2O_3 is the only iron-containing phase in the samples [34]. No hematite impurity was found. Thus, samples 05FS and 3FS can be considered as model ε-Fe_2O_3 nanoparticle systems without foreign phases.

The magnetic properties were examined using a vibrating sample magnetometer [35] in the temperature range of 4.2–300 K and a Quantum Design PPMS 6000 facility at temperatures above 300 K. The temperature dependences of the magnetization $M(T)$ at temperatures below 300 K were measured in the zero-field cooling (ZFC) and field cooling (FC) modes. The experimental data on magnetization are normalized to the Fe_2O_3 iron oxide mass.

Ferromagnetic resonance (FMR) spectra were obtained on a Bruker ELEXSYS 500 three-centimeter spectrometer operating in the X band.

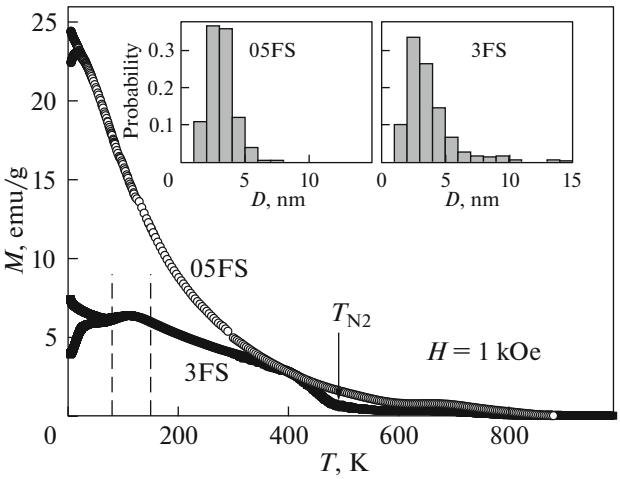

Fig. 1. Temperature dependences of magnetization for the investigated samples containing ε-Fe_2O_3 nanoparticles in the temperature range of 4.2–1000 K. Vertical dashed lines show the temperature range of the well-known magnetic transition in ε-Fe_2O_3. Inset: particle size distribution histograms for the investigated samples, according to the high resolution transmission electron microscopy data.

3. RESULTS AND DISCUSSION

3.1. Magnetization

Figure 1 shows temperature dependences of magnetization $M(T)$ for the samples in the range from 4.2 to 1000 K measured in an external field of H = 1 kOe. Let us consider first the $M(T)$ dependences obtained in the low-temperature range (Fig. 2). Sample 3FS is characterized by a nonmonotonic temperature dependence of magnetization in the range from 4.2 to 150 K (Fig. 2). The visible anomaly in the range of 80–150 K (shown by vertical dashed lines) corresponds to the well-known magnetic transition in ε-Fe_2O_3. At temperatures below 80 K, the strong effect of thermomagnetic history is observed. The magnetization of sample 05FS behaves differently: the monotonic magnetization growth with a decrease in temperature, the presence of a sharp $M(T)$ maximum under the ZFC conditions at 20 K, and effect of the thermomagnetic prehistory, which starts in the vicinity of 20 K. The maximum particle size in sample 05FS is no larger than 6 nm, and, as was shown in [28, 32], particles of such sizes do not undergo a magnetic transition in the range of 80–150 K. The observed ZFC $M(T)$ maximum corresponds to the superparamagnetic blocking temperature T_B (according to our data, the T_B value shifts toward lower temperatures as the external field increases).

The temperature dependence of magnetization for sample 05FS above the blocking temperature (Figs. 1, 2) is caused by the paraprocess characteristic of the superparamagnetic state, in which the $M(T)$ dependence is usually proportional to $1/T$. In sample 3FS,

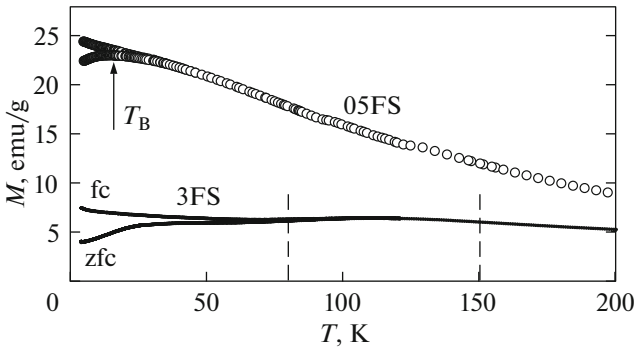

Fig. 2. Temperature dependences of magnetization for the investigated samples with different thermomagnetic prehistories in the low-temperature range (4.2–200 K). Vertical dashed lines show the temperature range of the well-known magnetic transition in ε-Fe_2O_3. The superparamagnetic blocking temperature T_B for sample 05FS is indicated.

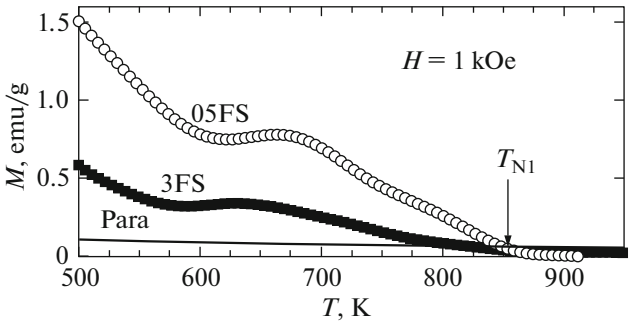

Fig. 3. Temperature dependences of magnetization for the investigated samples in the high-temperature (500–1000 K) region (symbols). The solid line shows the expected contribution of iron(III) ions in the paramagnetic state. The temperature T_{N1} of the transition to the paramagnetic state is shown.

on the contrary, most particles remain in the blocked state up to high (~500 K) temperatures, which results in the $M(T)$ dependence typical of ferromagnets (Fig. 1). One can see a sharp decrease in magnetization around 500 K (T_{N2} in Fig. 1). This feature undoubtedly corresponds to the magnetic transition, which was previously considered to be a transition to the paramagnetic state.

In addition, Fig. 1 shows that, at high (above 500 K) temperatures, the magnetizations of samples 05FS and 3FS are not vanishingly small. Figure 3 shows the smoothed $M(T)$ dependences for the investigated samples at high temperatures. The experimental magnetization values significantly exceed the response expected from iron atoms in Fe_2O_3 in the paramagnetic state in a field of $H = 1$ kOe calculated using the Brillouin function (line in Fig. 3). This implies the existence of a magnetic order in ε-Fe_2O_3 at high temperatures. According to the data in Fig. 3, the temperature of the transition to the paramagnetic state, which is denoted as T_{N2}, is about 850 K for both investigated samples. This is consistent with the data from [30].

As was mentioned above, for sample 05FS, no anomalies around 500 K are observed. This fact, along with the absence of a magnetic transition in the range of 80–150 K, evidences for a modified magnetic structure of the ε-Fe_2O_3 particles smaller than 6 nm. The analysis of the Mössbauer spectra of this sample disclosed a significant difference of the distribution of cationic positions from the ideal ordered ε-Fe_2O_3 structure [1]: the occupancy of tetrahedral positions becomes much higher [28]. This is, most likely, due to the defectness of the structure of ε-Fe_2O_3 particles with such a small size. However, it can be seen in Fig. 3 that the temperature of the transition to the paramagnetic state for sample 05FS is also about 850 K.

3.2. Ferromagnetic Resonance

Typical FMR spectra of the investigated samples recorded at different temperatures are shown in Fig. 4. In these spectra, a narrow intense absorption line is observed, which points out the presence of particles in the superparamagnetic state in the sample.

For an ensemble of single-domain magnetic particles in the superparamagnetic state, one may assume that the integral intensity of the FMR absorption signal is proportional to the saturation magnetization [36]. Figure 5 shows temperature dependences of the integral intensity of the FMR spectra for samples 05FS and 3FS. In both samples, the FMR spectrum is observed up to high temperatures, which shows the presence of magnetic ordering in the samples under study at high temperatures. In this case, the general form of the dependence agrees well with the magnetic measurement data (Fig. 3).

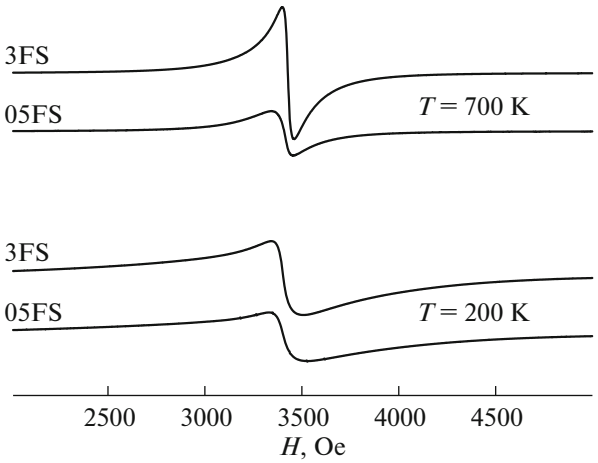

Fig. 4. FMR spectra for the investigated samples at different temperatures.

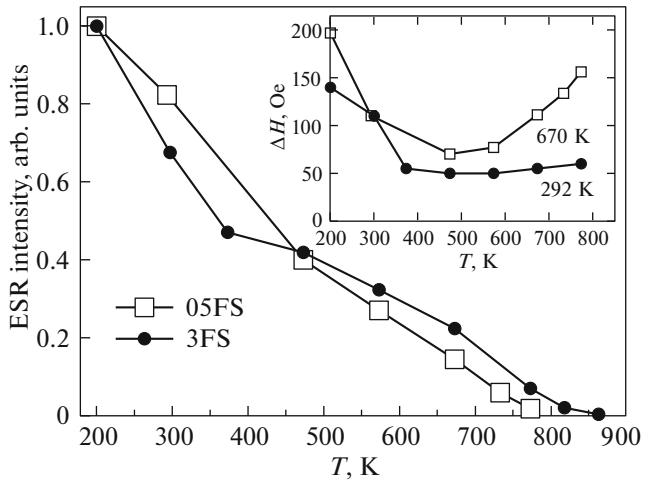

Fig. 5. Temperature dependences of the integral intensity of the FMR spectra of the investigated samples in the temperature range of up to 900 K. Inset: linewidths ΔH of the FMR spectra as a function of temperature.

The inset in Fig. 5 shows temperature dependences of the FMR linewidth ΔH. In the general case, the absorption linewidth for an individual single-domain particle depends on the crystallographic anisotropy, shape, and resonance conditions. However, when an ensemble of superparamagnetic particles is involved in the FMR spectrum formation, a great number of parameters are averaged due to heat fluctuations [37–39]. This leads, among other things, to averaging of local inhomogeneities in the sample and a decrease in the linewidth with increasing temperature (inset in Fig. 5). However, in the samples under study, the character of the $\Delta H(T)$ dependence at temperatures above 500 K qualitatively changes. This may indirectly indicate a change in the ε-Fe_2O_3 magnetic order.

4. CONCLUSIONS

Thus, the measurements of magnetization and temperature evolution of the FMR spectra of the investigated samples containing ε-Fe_2O_3 nanoparticles without other iron oxide polymorph admixtures showed the existence of a high-temperature magnetically ordered phase in ε-Fe_2O_3, which is consistent with the conclusions made in [30]. The magnetic order is retained up to a temperature of ~850 K and observed also in particles several nanometers in size.

ACKNOWLEDGMENTS

This study was supported by the Russian Science Foundation, project no. 17-12-01111.

REFERENCES

1. E. Tronc, S. Chaneac, and J. P. Jolivet, J. Solid State Chem. **139**, 93 (1998).
2. M. Gich, A. Roig, C. Frontera, E. Molins, J. Sort, M. Popovici, G. Chouteau, D. Martın Marero, and J. Nogues, J. Appl. Phys. **98**, 044307 (2005).
3. M. Popovici, M. Gich, D. Nińanský, A. Roig, C. Savii, L. Casas, E. Molins, K. Zaveta, C. Enache, J. Sort, S. de Brion, G. Chouteau, and J. Nogués, Chem. Mater. **16**, 5542 (2004).
4. V. N. Nikolić, M. Tadić, M. Panjan, L. Kopanja, N. Cvjetićanin, and V. Spasojević, Ceram. Int. **43**, 3147 (2017).
5. V. N. Nikolić, V. Spasojević, M. Panjan, L. Kopanja, A. Mraković, and M. Tadić, Ceram. Int. **43**, 7497 (2017).
6. D. A. Balaev, S. S. Yakushkin, A. A. Dubrovskii, G. A. Bukhtiyarova, K. A. Shaikhutdinov, and O. N. Mart'yanov, Tech. Phys. Lett. **42**, 347 (2016).
7. E. Tronc, C. Chaneac, J. P. Jolivet, and J. M. Greneche, J. Appl. Phys. **98**, 053901 (2005).
8. M. Kurmoo, J.-L. Rehspringer, A. Hutlova, C. D'Orlans, S. Vilminot, C. Estournes, and D. Niznansky, Chem. Mater. **17**, 1106 (2005).
9. M. Gich, C. Frontera, A. Roig, E. Taboada, E. Molins, H. R. Rechenberg, J. D. Ardisson, W. A. A. Macedo, C. Ritter, V. Hardy, J. Sort, V. Skumryev, and J. Nogués, Chem. Mater. **18**, 3889 (2006).
10. J. Tućek, R. Zboril, A. Namai, and S. Ohkoshi, Chem. Mater. **22**, 6483 (2010).
11. L. Machala, J. Tućek, and R. Zboril, Chem. Mater. **23**, 3255 (2011).
12. J. Jin, S. Ohkoshi, and K. Hashimoto, Adv. Mater. **16**, 48 (2004).
13. S. Ohkoshi, S. Sakurai, J. Jin, and K. Hashimoto, J. Appl. Phys. **97**, 10K312 (2005).
14. S. Sakurai, J. Shimoyama, K. Hashimoto, and S. Ohkoshi, Chem. Phys. Lett. **458**, 333 (2008).
15. S. Sakurai, A. Namai, K. Hashimoto, and S.-I. Ohkoshi, J. Am. Chem. Soc. **131**, 18299 (2009).
16. S. Ohkoshi, S. Kuroki, S. Sakurai, K. Matsumoto, K. Sato, and S. Sasaki, Angew. Chem. Int. Ed. **46**, 8392 (2007).
17. A. I. Dmitriev, O. V. Koplak, A. Namai, H. Tokoro, S. Ohkoshi, and R. B. Morgunov, Phys. Solid State **56**, 1795 (2014).
18. A. I. Dmitriev, O. V. Koplak, A. Namai, H. Tokoro, S. Ohkoshi, and R. B. Morgunov, Phys. Solid State **55**, 2252 (2013).
19. A. I. Dmitriev, Tech. Phys. Lett. **44**, 137 (2018).
20. A. Namai, M. Yoshikiyo, K. Yamada, S. Sakurai, T. Goto, T. Yoshida, T. Miyazaki, M. Nakajima, T. Suemoto, H. Tokoro, and S. Ohkoshi, Nat. Commun. **3**, 1035 (2012).
21. S. Ohkoshi, A. Namai, T. Yamaoka, M. Yoshikiyo, K. Imoto, T. Nasu, S. Anan, Y. Umeta, K. Nakagawa, and H. Tokoro, Sci. Rep. **6**, 27212 (2016).
22. S. Ohkoshi, A. Namai, M. Yoshikiyo, K. Imoto, K. Tamazaki, K. Matsuno, O. Inoue, T. Ide, K. Masada, M. Goto, T. Goto, T. Yoshida, and T. Miyazaki, Angew. Chem. **128**, 11575 (2016).

23. M. Nakaya, R. Nishida, N. Hosoda, and A. Muramatsu, Cryst. Res. Technol. **52**, 1700110 (2017). doi 10.1002/crat.201700110

24. S. S. Yakushkin, D. A. Balaev, A. A. Dubrovskiy, S. V. Semenov, Yu. V. Knyazev, O. A. Bayukov, V. L. Kirillov, R. D. Ivantsov, I. S. Edelman, and O. N. Martyanov, Ceram. Int. **44**, 17852 (2018). doi 10.1016/j.ceramint.2018.06.254

25. G. A. Bukhtiyarova, M. A. Shuvaeva, O. A. Bayukov, S. S. Yakushkin, and O. N. Martyanov, J. Nanopart. Res. **13**, 5527 (2011).

26. S. S. Yakushkin, G. A. Bukhtiyarova, and O. N. Martyanov, J. Struct. Chem. **54**, 876 (2013).

27. O. S. Ivanova, R. D. Ivantsov, I. S. Edelman, E. A. Petrakovskaja, D. A. Velikanov, Y. V. Zubavichus, V. I. Zaikovskii, and S. A. Stepanov, J. Magn. Magn. Mater. **401**, 880 (2016).

28. A. A. Dubrovskiy, D. A. Balaev, K. A. Shaykhutdinov, O. A. Bayukov, O. N. Pletnev, S. S. Yakushkin, G. A. Bukhtiyarova, and O. N. Martyanov, J. Appl. Phys. **118**, 213901 (2015).

29. D. A. Balaev, I. S. Poperechny, A. A. Krasikov, K. A. Shaikhutdinov, A. A. Dubrovskiy, S. I. Popkov, A. D. Balaev, S. S. Yakushkin, G. A. Bukhtiyarova, O. N. Martyanov, and Yu. L. Raikher, J. Appl. Phys. **117**, 063908 (2015).

30. J. L. Garcıa-Muñoz, A. Romaguera, F. Fauth, J. Nogués, and M. Gich, Chem. Mater. **29**, 9705 (2017).

31. S. S. Yakushkin, A. A. Dubrovskiy, D. A. Balaev, K. A. Shaykhutdinov, G. A. Bukhtiyarova, and O. N. Martyanov, J. Appl. Phys. **111**, 44312 (2012).

32. D. A. Balaev, A. A. Dubrovskiy, K. A. Shaykhutdinov, O. A. Bayukov, S. S. Yakushkin, G. A. Bukhtiyarova, and O. N. Martyanov, J. Appl. Phys. **114**, 163911 (2013).

33. G. A. Bukhtiyarova, O. N. Mart'yanov, S. S. Yakushkin, M. A. Shuvaeva, and O. A. Bayukov, Phys. Solid State **52**, 826 (2010).

34. S. S. Yakushkin, D. A. Balaev, A. A. Dubrovskiy, S. V. Semenov, K. A. Shaikhutdinov, M. A. Kazakova, G. A. Bukhtiyarova, O. N. Martyanov, and O. A. Bayukov, J. Supercond. Nov. Magn. **31**, 1209 (2017).

35. A. D. Balaev, Yu. V. Boyarshinov, M. M. Karpenko, and B. P. Khrustalev, Prib. Tekh. Eksp., No. 3, 167 (1985).

36. G. V. Skrotskii and L. V. Kurbatov, in *Ferromagnetic Resonance, Collection of Articles*, Ed. by S. V. Vonsovskii (Fizmatlit, Moscow, 1961), p. 25 [in Russian].

37. R. S. de Biasi and T. C. Devezas, J. Appl. Phys. **49**, 2466 (1978).

38. R. Berger, J. Kliava, J. C. Bissey, and V. Baietto, J. Appl. Phys. **87**, 7389 (2000).

39. Yu. L. Raikher and V. I. Stepanov, Phys. Rev. B **50**, 6250 (1994).

Translated by E. Bondareva